Ice melting and earthquake suppression in Greenland

M. Olivieri[a,*], G. Spada[b]

[a] *Istituto Nazionale di Geofisica e Vulcanologia, Sezione di Bologna, via Donato Creti 12, 40128 Bologna, Italy*

[b] *Dipartimento di Scienze di Base e Fondamenti (DiSBeF), Università di Urbino "Carlo Bo", Urbino, Italy*

Abstract

It has been suggested that the Greenland ice sheet is the cause of earthquake suppression in the region. With few exceptions, the observed seismicity extends only along the continental margins of Greenland, which almost coincide with the ice sheet margin. This pattern has been put forward as further validation of the earthquake suppression hypothesis. In this review, new evidence in terms of ice melting, post-glacial rebound and earthquake occurrence is gathered and discussed to re-evaluate the connection between ice mass unloading and earthquake suppression. In Greenland, the spatio-temporal distribution of earthquakes indicates that seismicity is mainly confined to regions where the thick layer of ice is absent and where significant ice melting is presently occurring. A clear correlation between seismic activity and ice melting in Greenland is not found. However, earthquake locations and corresponding depth distributions suggest two distinct governing mechanisms: post-glacial rebound promotes moderate-size crustal earthquakes at Greenland's regional scale, while current ice melting promotes shallow low magnitude seismicity locally.

Keywords: *Greenland, Earthquakes, Ice sheet melting*

1. Introduction

In the framework of plate tectonics, earthquake locations and corresponding focal mechanisms define the location of plate boundaries and their types. In the simplest scenario, this was considered as evidence in support of the rigid behavior of plates (Morgan, 1968). Some earthquakes, however, occur in the plate interior, showing that indeed plates are not totally rigid. Some of these so-called intraplate earthquakes stand out and can reach magnitudes as large as $M_w = 8$ (Gordon, 1998; Nettles et al., 1999; Gupta et al., 2001). Various mechanisms have been invoked to explain the origin of intraplate earthquakes; these essentially involve the horizontal transmission of stress through the lithospheric plates and its gradual accumulation along preexisting faults or weak zones far from the plate boundaries. Stress migration is supported by the relation between intraplate deformation and the seismicity in stable continental regions (SCRs) (see, e.g., Stein and Mazzotti, 2007).

Intraplate earthquakes can also originate from processes that do not involve the horizontal movement of plates. As first suggested by Gutenberg and Richter (1954), post-glacial rebound (PGR) in response to the melting of the late-Pleistocene ice sheets (e.g., Turcotte and Schubert, 2002) is a viable candidate for intraplate seismicity. PGR has caused, and it is presently causing, vertical and horizontal crustal deformation at high latitude regions, inducing stress variations within the lithosphere and the mantle (Spada et al., 1991). Wu and Johnston (2000) pointed out that ice unloading may be the cause of seismicity at the ice margins and that this was

*Corresponding author
Email address: marco.olivieri@bo.ingv.it (M. Olivieri)

possibly the cause of paleo-earthquakes in Charlevoix (Quebec) and in the Wabash Valley (IN, USA). Recently, Brandes et al. (2012) have pointed to a glacial origin for the 1612 Bielefeld (Germany) earthquake, which occurred along the so-called Osning Thrust system. A similar case was identified in Sweden, where rapid ice retreat during the Pleistocene-Holocene transition was related to the occurrence of the $M = 7.5$ Lake Vättern earthquake (Jakobsson et al., 2014). Although the four large earthquakes of 1811–1812 in New Madrid (MO, USA) have been quoted in the literature as an example of PGR-induced earthquakes, Wu and Johnston (2000) concluded that "glacial unloading is unlikely to have triggered the large $M = 8$ earthquakes in New Madrid" (see also Hough et al., 2000). Wu and Johnston found that the load-induced stress field variations decay rapidly outside the ice margins and their amplitude is too small to generate earthquakes of this size. As suggested by Calais et al. (2010), the New Madrid earthquakes could have been triggered by rapid uplift in response to erosion along the Mississippi River, rather than being directly associated with deglaciation. The Gutenberg and Richter (1954) hypothesis about the role of PGR is now supported by modeling efforts aimed to explain the post-glacial origin of earthquakes (Steffen et al., 2014a).

In their earthquake catalogue for SCRs for the period 495–2003, Schulte and Mooney (2005) have included $M > 4.5$ earthquakes in all the SCRs identified worldwide. None is identified in Greenland, although evidence of paleo-seismicity and historical earthquakes can hardly be retrieved from remote regions or where a tradition for written records is lacking. For Greenland, before the advent of modern seismology, descriptions of felt earthquakes are only available since the second half of the 17^{th} century

(Gregersen, 1982). PGR is mentioned by Schulte and Mooney (2005) as one of the possible causes of earthquakes in SCRs. However, the role of PGR in the triggering of seismicity in deglaciated areas was proposed by various authors (see e.g., Stein et al. 1979, Quinlan 1984, for the case of Canada). Muir-Wood (2000) suggested a more complex mechanism of stress and strain interaction in deglaciated areas. The important role of PGR in the stress redistribution across deglaciated areas was later demonstrated by Steffen et al. (2012) and Steffen et al. (2014a) with reference to the cases of Greenland and Antarctica.

In seminal work "Suppression of earthquakes by large continental ice sheets", Johnston (1987) suggested that the aseismicity of Greenland and Antarctica could be due to "pressure effects produced by the continental ice sheets that mantle both continents", an idea stemming from studies of seismicity induced by water reservoirs and dams. Chung (2002) discussed the connection between PGR and seismicity along passive continental margins, showing that the focal mechanisms of the largest recorded earthquakes correspond to normal faults in a horizontal extension environment. Chung (2002) confirmed previous results from Chung and Gao (1997) about the seismicity in deglaciated areas and concluded that seismicity is spatially correlated with deglaciated areas of the Greenland ice sheet (GrIS) located along passive continental margins. These mark the watershed between earthquake occurrence outside the ice sheet and quiescence beneath. When the works by Johnston (1987) and Chung and Gao (1997) were published, ongoing massive ice melting in Greenland was not yet observed (Alley et al., 2010) and the possible role of ice unloading as a cause of seismicity was only mentioned in passing by these authors.

Twenty-five years after the publication of the work by Johnston (1987), the continental ice sheets are globally thinner and lighter (Meehl et al., 2007), various estimates of the mass balance of the GrIS exist (Alley et al., 2010) and high-resolution models for the on-going ice mass loss in Greenland have been obtained by space-geodetic techniques (Velicogna and Wahr, 2005; Sørensen et al., 2011). Furthermore, we now have more detailed earthquake datasets from the deployment of dense seismological networks (Dahl-Jensen et al., 2010). Recently, efforts by the Greenland Ice Sheet Monitoring Network (GLISN) consortium have improved the spatial coverage by state-of-the-art seismic stations (Clinton et al., 2014), leading to an increased capability of earthquake detection and localization and to a better understanding of the origin of icequakes (Nettles and Ekström, 2010; Walter et al., 2013). The seismic characterization of calving events in Greenland now facilitates the discrimination between tectonic and ice-related earthquakes (Walter et al., 2009). The thick ice sheet hampers the interpretation of geological features whose observation is confined to the margins of the Greenland craton (see Escher and Pulvertaft, 1995 and references therein). Greenland, however, can be considered stable and presently subject to little tectonic deformation.

The aim of this work is to discuss the possible relationship between ice melting in Greenland and the spatio-temporal distribution of seismicity. We first describe a model for the mass balance of the GrIS during the last decade. Then, we introduce the earthquake catalogue and we analyze the seismicity at regional (i.e., Greenland scale) and local scales, focusing on the sectors currently subject to ice wastage. Lastly, we discuss the relationship between deglaciation and the occurrence of earthquakes making use of recent

models by Steffen et al. (2014a).

2. Present melting of the GrIS

Estimates of the total mass balance of the GrIS are based on a broad range of techniques. In their review, Alley et al. (2010) have collected mass balance estimates from various sources (see their Figure 2). It is apparent that during 1995–2000, a significant acceleration of the mass loss of the GrIS has been observed, which roughly corresponded to a marked increase of coastal temperatures. Recent observations by gravimetry and altimetry, relative to the period 2000–2012, point to a time-averaged mass balance in the range between -200 and -250 Gt yr^{-1}, i.e. ~ 3 times in excess of those inferred during 1960–2000 (Alley et al., 2010).

Figure 1a shows the total mass balance of the GrIS for the period 2003– 2008 according to Sørensen et al. (2011), expressed in units of meters of ice loss (or gain) per year. The mass balance has been obtained from repeated surface elevation observations from NASA's Ice Cloud and land Elevation Satellite (ICESat, see *http://icesat.gsfc.nasa.gov/*), which operated from 2002 to 2009 and provided a unique data set for cryospheric studies. Since altimetry alone is not sufficient to provide an estimate of the mass balance, the rates of mass loss in Figure 1a have been recovered by modeling of the firn dynamics and surface ice densities. The figure corresponds to model M3 of Sørensen et al. (2011), which implies a rate of mass loss of 240 ± 28 Gt yr^{-1}. Mass balance M3 is in broad agreement with that based on observations from the NASA/DLR Gravity Recovery and Climate Experiment (GRACE) during the same time span of the ICESat observations (Schrama and Wouters, 2011).

F1a

The GrIS mass balance M3 has been recently employed by Spada et al. (2012) and Nielsen et al. (2014) to reconcile the Global Positioning System observations of vertical uplift to the ongoing elastic rebound (ER) in response to the GrIS melting and PGR. Compared to GRACE solutions, which provide the mass balance of the GrIS to a maximum harmonic degree 60 (see e.g., Schrama and Wouters 2011), M3 attains a much larger spatial resolution (the grid spacing is 5 km). This allows to clearly distinguish (Figure 1a) the regions subject to ice loss (blue hues), with rates exceeding 5 m yr^{-1} in the vicinity of Jakobshavn Isbræ (JI) in the west, of the Kangerdlugssuaq Glacier (KG), the Helheim Glacier (HG) and the Southeast Glaciers (SG) in the east. Very localized spots of ice accumulation (orange and red) are visible in the northeast near the Flade Isblink (FI) and the Storstrømmen (St), while the bulk of the GrIS is experiencing an ice accumulation rate of $\sim 0 - 0.5$ m yr^{-1} (Spada et al., 2012).

3. Observed seismicity

Figure 1b shows the distribution of seismicity in Greenland during the last 60 years according to the ISC catalogue (International Seismological Centre, 2011). The spatial distribution is consistent with the earthquake suppression hypothesis by Johnston (1987), although earthquake monitoring capability has changed dramatically in the last decades. This occurred as a consequence of the deployment of denser seismic networks (Clinton et al., 2014) and improvements in data transmission and processing (Olivieri and Clinton, 2012). Since the minimum detectable earthquake magnitude is continuously decreasing, the analysis of seismic catalogues deserves scrutiny. Using the concept of Magnitude of Completeness (hereafter M_c) (Rydelek F1b

and Sacks, 1989), it is possible to compare catalogues from different epochs. This allows to avoid misinterpretations of changes in the rates of seismicity, given that the detection capability depends on the spatio-temporal distribution of stations (Albarello et al., 2001).

To put the case study of Greenland in a global perspective, we first analyzed the changes in the occurrence of earthquakes at a global scale. We selected January 1988, immediately after the paper of Johnston (1987) was published, as a watershed. The aim is to establish whether regions exist where some significant seismic activity started after this date and if these correspond to any of the known SCRs. We use the ISC catalogue (International Seismological Centre, 2011) which merges seismic bulletins (including events and phases) from more than 130 agencies worldwide, and can be considered the most complete catalog at global and regional scales.

From the entire ISC catalogue, we have selected earthquakes with magnitude $M \geq 5.0$ and hypocentral depth < 30 km, a choice motivated by the characteristic magnitude and depth of the largest earthquakes observed in Greenland (see Table 1). Then, we counted the earthquakes that occurred T1
within $5^\circ \times 5^\circ$ rectangular pixels over the Earth surface both before and after 1988. Green pixels in Figure 2 show areas where at least one earth- F2
quake occurred before and after 1988, while for red ones one earthquake, at least, was recorded only after the same epoch. The distribution of red rectangles shows that "new seismicity" after 1988 was only observed in two cases, namely along remote plate boundaries which were not previously sufficiently covered by the network, or in the neighborhood of known seismic zones where events "migrated" as a consequence of improved location capability. However, Figure 2 also shows that, in the range of magnitudes

and hypocentral depths considered here, no earthquakes occurred inland Greenland or Antarctica, nor in the regions which were covered by thick layers of ice until a few thousands of years ago (Scandinavia and Canada). The "appearance" of seismicity in the southernmost tip of Greenland merits further attention.

3.1. Regional seismicity

The most comprehensive earthquake catalogue for Greenland (International Seismological Centre, 2011) includes 901 events for the time period 1951–2012. Information about these events are shown in Figure 1b. The largest reported magnitude is $m_b = 5.5$; only five events have magnitude $M \geq 5.0$. Four moment tensor solutions are available (see Table 1); all are characterized by normal fault mechanisms with strike planes approximately aligned with the continental margin (Sykes and Sbar, 1974; Dziewonski et al., 1981; Chung, 2002). For about 15% of the events (134 of the total blue dots in Figure 1b), no magnitude is available. In different epochs, earthquake magnitude was, and it still is, computed adopting different methods and attenuation laws. For this reason, here we will use the symbol M to indicate generic values of magnitude (for a comprehensive review about different types of magnitude, see paragraph 1.2.2.1 of Bormann, 2012 and references therein). Unfortunately, no relationships exist to convert from body-wave, surface-wave and moment magnitude to local magnitude. This prevents the creation of an homogeneous earthquake catalogue for Greenland, which would be necessary for a rigorous analysis of the magnitudes distribution over time. For these reasons, when more than one magnitude estimate is available, we use the one preferred in the ISC catalogue since

the lack of additional information prevents a different approach.

By reconstructing a Gutenberg and Richter (1944) relationship, we estimated M_c for the seismicity of Greenland. According to the diagram in Figure 3a, we find $M_c = 4.0$, which provides an empirical estimate of the magnitude threshold above which all the occurred earthquakes are inferred to have been detected. The available dataset does not match the requirements for a state-of-the-art analysis as described by Woessner and Wiemer (2005), which allows to study the spatial pattern of M_c and also to obtain estimates for the associated errors. Of course, M_c is meaningless for those areas of Greenland in which seismicity is absent or not observed. F3a

Most of the earthquakes in Figure 1b, and all but one above M_c, are located along the margins of the GrIS, which roughly correspond to the continental margins, as previously observed by Sykes (1978). The only exception is the earthquake that occurred on 1975/12/22 ($m_b = 4.6$), highlighted in Figure 1b. The poor azimuthal coverage of the epicentral solution and the fact that this earthquake is not in the catalogue published by NORSAR (*http://www.norsardata.no/NDC/bulletins/norsar*) makes us suspicious about the possible mislocation of this earthquake. By visual inspection of several months of data for station GE.SUMG (located at the Summit, Central Greenland) during time period 2011–2012, we could not observe any additional local seismicity emerging from the noise.

The significant changes in the seismic network density in Greenland over the time span covered by the catalogue, require us to verify if M_c consequently changed over time. However, the consequences of network changes in Greenland are mitigated by the fact that earthquakes of magnitude $M = 4.0$ and above are also detected at stations and arrays located in

the surrounding countries (e.g. ARCES and NORES in Norway).

To provide an estimate of how M_c has been changing over time at regional scale, we have implemented a slight modification of the recipe by Mignan and Woessner (2012). From the complete catalogue, we picked groups of 50 events in temporal sequence, with each group sharing the first 20 events with the last 20 of the previous. For each group we computed M_c. Then, we assigned to each M_c a time stamp that corresponds to the median of the time span over the bin. The reduction of the number of events in each bin from 250 as used by Mignan and Woessner (2012) to only 50 events, is motivated by the smaller number of low magnitude earthquakes in our catalogue. The results are gathered in Figure 4a where M_c values are shown as a function of time. A value $M_c = 4$ is obtained already at the beginning of the time window (year 1969). F4a

As mentioned above, earthquake rates are strongly dependent on the detection threshold and this effect is clearly perceivable in Figure 3b, where earthquake occurrence for the entire catalogue is represented by two-years long bins. The catalogue restricted to earthquakes with $M \geq M_c$ (hereafter referred to as Catalogue$_c$) is more suitable for the purpose of interpreting rates of seismicity over time. Catalogue$_c$ contains 75 earthquakes during the period 1969–2012 and is displayed in Figure 3c in terms of number of earthquakes binned per year. The figure also shows the cumulative distribution $C_c(t)$ (thick curve), defined as the number of earthquakes occurred until time t. F3b

To quantitatively estimate possible variations in the rate of seismicity at Greenland's regional scale, we use the method of Olivieri and Spada (2013) to analyze the trend of global sea-level curves. In particular, by means of a

Fisher F-test (Winer, 1962), we compared quadratic and bilinear regression models for $C_c(t)$ with that assuming a constant rate of seismicity. We find that, for curve $C_c(t)$, the best-fitting regression model is bilinear (95% confidence), characterized by a change point in mid 1993 which marks an increase of the rate of earthquakes from 1.33 ± 0.02 to 1.83 ± 0.05 events per year. Earthquakes are expected to result from a Poisson process, which puts in the shade the statistical significance of variations in the temporal distribution of earthquakes in catalogues (Shearer and Stark, 2012).

The evaluation of the statistical significance for temporal variations We have simulated 10^5 catalogues with the same number of events and time span equal to that of Catalogue$_c$ and we have verified that, with a 95% of confidence, the distribution of events before and after the change point does not result from an homogeneous Poisson process. This further confirms a change in the rate of seismicity at Greenland's regional scale around 1993.

3.2. Local seismicity

From Figures 1a and 1b it appears that regions of relatively intense seismicity correspond to places which undergone significant ice wasting during last decades. In this respect, three sectors are of particular interest. The local seismicity across these sectors, labeled by W, Se and N in Figure 1a, is separately considered in Figures 5a, 6a and 7a, respectively. Sector W includes the Jakobshavn Isbræ, Se encompasses the Helheim and Southern Glaciers, three of the glaciers that have experienced faster retreat in the last decades (Moon et al., 2012), while N also includes glaciers that are currently gaining mass (Spada et al., 2012). The epicenters of the largest earthquakes in Greenland (Table 1) are located in sectors Se and N. Sectors

F5a F6a F7a

W and Se also experienced intense seismicity in the period 2009–2012, in the range of 50 to 150 earthquakes per year (Figures 5b and 6b). For sector Se, in particular, there are some reports for felt earthquakes in the vicinity of Tasiilaq (Larsen et al., 2014). Analysis of the local earthquakes in the Ammassalik region in sector Se has shown alignment of hypocentres with geological boundaries (Pinna and Dahl-Jensen, 2012). F5b F6b

For each of the three sectors we analyzed Catalogue$_c$ over time as described in Section 3.1, in order to retrieve the minimum M_c valid for the longest time span according to the existing dataset. The results are plotted in Figure 4 and are summarized in Table 2 together with those for entire Greenland. We find that M_c is almost consistent with that observed at regional scale: $M_c = 4.0$ for sectors N and Se; while in sector W we find $M_c = 3.9$. However, the time span of validity for the obtained M_c varies considerably. In sector N the validity of M_c extends back to 1976. For sector W and Se, the M_c value obtained is only valid since 1999 and 2002, respectively. This limits the detectability of temporal variations in the rate of seismicity. T2

For each sector, we display seismicity over time in terms of magnitude (see Figures 5b, 6b and 7b). Note that in all these figures, seismicity below the M_c threshold for each sector, marked by an horizontal line, only appears since $\sim$ 2009. This is a consequence of the deployment of new seismic stations enabling the detection of local earthquakes. The same statistical analysis described above for $C_c(t)$ is repeated here for each of the three sectors W, N and Se, analyzing the cumulative functions $C_c^W(t)$, $C_c^N(t)$ and $C_c^{Se}(t)$ shown by bold lines in Figures 5c, 6c and 7c, respectively. In the same plots, the histograms show the number of events with magnitude F7b F5c F6c F7c

315 $M \geq M_c$ in the whole time window. The outcome of the analysis of the
316 cumulative functions is summarized in Table 2. Contrary to what we ob-
317 served at Greenland's regional scale in Section 3.1, we find no evidence, in
318 any of the sectors, for an increase in the rate of seismicity over the analyzed
319 time-span. Significantly, in sector N the best-fitting relation is bilinear with
320 a decrease of the rate of seismicity from (0.93 ± 0.04) to (0.49 ± 0.03) events
321 per year. Our method of searching for a bilinear best-fit does not impose
322 continuity at the change point (Chow, 1960). Thus, the decreasing rate
323 could be an artifact caused by the apparent large number of earthquakes in
324 1993.

325 4. Discussion and conclusions

326 The available geological and seismological observations support the idea
327 that Greenland sits on an old and stable continental platform, where no
328 large active faults have been recognized. The seismicity of Greenland is
329 classified as intraplate seismicity and it is confined to the margins of the
330 continental crust (see Figure 1a).

331 Currently, Greenland is subject to significant deformation in response
332 to the present-day melting of the GrIS (the "elastic rebound", ER) and
333 to the PGR resulting from the late-Pleistocene deglaciation. These two
334 processes, which are acting simultaneously, have been analyzed by Spada
335 et al. (2012) in the context of Greenland. To depict the ER effects, in
336 Figure 8a we have shown the pattern of vertical uplift rate associated with F8a
337 the mass balance M3 of Figure 1. This rate is constant within the time
338 window of the ICESat observations employed to obtain the mass balance
339 (namely, from 2002 to 2009, see Sørensen et al. 2011). In regions where

glaciers experience significant ice mass loss, the uplift rate widely exceeds 20 mm yr^{-1} (Spada et al., 2012). The PGR in terms of crustal uplift rate, shown in Figure 8b and obtained from Peltier (2004), attains the largest values in the North and a local maximum also at the southern tip, with rates not exceeding 10 mm yr^{-1} across Greenland. F8b

According to all the seismological information currently available for period 1951–2012 and displayed in Figure 1b, we observe that the interior of Greenland persists in being essentially aseismic in this time span. This is corroborated by inspection of data from the GE.SUMG station (the Summit) and by the 2013 online catalogue by Geological Survey of Denmark and Greenland (GEUS, *http://seis.geus.net/projects/glisn/ geus-eqlist.html*). The observed seismicity is confined to the margins of the GrIS and approximately follows the coastlines. These findings are consistent with those of Johnston (1987), Chung and Gao (1997) and Chung (2002).

In the aseismic central portion of Greenland, the rate of crustal uplift associated with the ER process is basically counterbalanced by that of PGR (Figure 8). In some cases, the clustering of seismicity is matching local maxima of the uplift pattern. This occurs in the southern tip of Greenland, where both ER and PGR concur to produce sizable uplift rates, in the W sector where ER largely dominates PGR and in the N sector, where PGR is dominating ER. However, in the seismically quiescent northwest significant PGR effect is discerned. Since the time-variations of the loading-induced stress fields at depth have not been evaluated here, this spatial correlation cannot be corroborated by a more rigorous study and these contradictory spatial observations do not help to discriminate the possible source mechanism for the observed seismicity.

ER and PGR have different time scales: the first was observed for the period 2003–2009 and different studies support the hypothesis that it started at the end of last century (see Alley et al., 2010 and references therein). On the contrary, PGR evolves on the millennium time scales and during last century the associated rates of deformation have been approximately constant. At regional scale we have observed a change in the rate of occurrence for earthquakes for the time period 1969–2012. This is best fitted by a sudden acceleration in $\sim$ 1993. When looking at the local scale, in sectors Se and W we do not observe any change in the rate of seismicity, but the short time span (10 and 12 years, respectively) limits the capability of detecting any change. In sector N, where the time span is longer (36 years), we observe a decrease in the long-term rate of seismicity, but we also note seismicity above the average for year 1993. In this context, the significance of the earthquake with $M \geq 5$ at the southernmost tip shown in Figure 2 remains unclear.

The consideration above suggest the existence of distinct types of seismicity: one kind being triggered by PGR and the other by ER. Some authors (e.g., Sauber and Molnia, 2004) analyzed the stress induced by the ice fluctuations at the glacier terminus and concluded that this can be the cause of shallow ($h \leq 5$ km) seismicity. Inspecting our catalogue, we find 30% of the total, but only 8% of those in Catalogue$_c$, with depth ≤ 5 km. Low magnitude seismicity is dominated by shallow depth events, while the moderate events occur at larger depth. Therefore, we can only speculate about the existence of two distinct mechanisms that cause the observed seismicity in Greenland: PGR that induces crustal earthquakes with moderate magnitude and ice melting that causes shallow small magnitude seismicity. At

present, more robust and unambiguous conclusions cannot be drawn, since the spatio-temporal limitations of the available data sets (earthquakes and ice mass change) limit our analysis to a phenomenological level.

Quantitative models as those proposed by Hampel and Hetzel (2006) and Steffen et al. (2014a,b) shed new light about the connection between PGR, ER and seismicity in deglaciated areas. In particular, the finite-element model by Steffen et al. (2014a) addresses quantitatively the problem of faults activation in response to ice unloading. Large paleo-earthquakes usually show large dip angle thrust fault mechanisms (Steffen et al., 2014a and references therein) while Quinlan (1984) observed that PGR-related stresses are normally too low to create new faults. The model by Steffen et al. (2014a) focuses on the re-activation of thrust faults at different distances from the center of the deglaciated region. The case of Greenland fits the reference model of Steffen et al. (2014a) well in terms of crustal and lithospheric thickness (Braun et al., 2007; Darbyshire et al., 2004) and maximum thickness of the ice sheet at the Last Glacial Maximum (Tushingham and Peltier, 1991). The model predicts the occurrence of one or two large earthquakes at the end of the deglaciation phase and 1 kyr later, depending on the possible dip angle of the fault. At the continental margin of Greenland, the degliaciation ended almost 5 kyrs before present (Tushingham and Peltier, 1991). Therefore, the moderate normal fault earthquakes observed in the last decades (see Figure 1) can be hardly interpreted, as the result of PGR since timing and the fault mechanism do not agree with the model prediction. More likely, the ongoing seismicity could be part of what the authors call the "post seismic phase" following the PGR-induced earthquake.

Some questions remain which would require further study in terms of data analysis and modeling. In particular, the observed normal fault mechanisms in Greenland appear to be in contrast with the earthquakes predicted by Steffen et al. (2014a) even though these observations are consistent with other models of PGR-induced seismicity. Paleo-earthquake records would possibly shed new light on the initiation of the ongoing seismic quiescence in continental Greenland. The search for these records could take advantage of recent high resolution observations of the bedrock beneath the GrIS (Bamber et al., 2013). Lastly, improved earthquake focal solutions and consistent magnitude estimates for the contemporary seismicity would provide useful constraints for theoretical models.

5. Acknowledgments

We thank Rebekka Steffen for very constructive comments, two anonymous reviewers for insightful suggestions,and the Editor-in-Chief Kazuo Shibuya for advice. We are indebted to Thorsten Becker who copy-edited the manuscript and provided useful comments. Earthquake catalogs have been extracted from the ISC (International Seismological Centre) archive on September 17, 2013 (*http://www.isc.ac.uk*). The GE.SUMG station is maintained by the GEOFON network (Hanka et al., 2010) and data were retrieved on August 10, 2013 from the WebDC portal (*http://www.webdc.eu*). All figures were made using the GMT package of Wessel and Smith (1998). Data for model ICE-5G(VM2) of Peltier (2004) are obtained from page *http://www.atmosp.physics.utoronto.ca/∼peltier/data.php*. The Norsar catalogue for teleseismic earthquakes was accessed Jul 8, 2014.

6. References

Albarello, D., Camassi, R., Rebez, A., 2001. Detection of space and time heterogeneity in the completeness of a seismic catalog by a statistical approach: an application to the Italian area. Bulletin of the Seismological Society of America 91 (6), 1694–1703.

Alley, R. B., Andrews, J. T., Brigham-Grette, J., Clarke, G., Cuffey, K., Fitzpatrick, J., Funder, S., Marshall, S., Miller, G., Mitrovica, J., et al., 2010. History of the Greenland ice sheet: paleoclimatic insights. Quaternary Science Reviews 29 (15), 1728–1756.

Bamber, J. L., Siegert, M. J., Griggs, J. A., Marshall, S. J., Spada, G., 2013. Paleofluvial mega-canyon beneath the central Greenland ice sheet. Science 341 (6149), 997–999.

Bormann, P., 2012. New Manual of Seismological Observatory Practice (NMSOP-2). IASPEI, GFZ German Research Centre for Geosciences, Potsdam.

Brandes, C., Winsemann, J., Roskosch, J., Meinsen, J., Tanner, D. C., Frechen, M., Steffen, H., Wu, P., 2012. Activity along the Osning Thrust in Central Europe during the Lateglacial: ice-sheet and lithosphere interactions. Quaternary Science Reviews 38, 49–62.

Braun, A., Kim, H. R., Csatho, B., von Frese, R. R., 2007. Gravity-inferred crustal thickness of Greenland. Earth and Planetary Science Letters 262 (1), 138–158.

Calais, E., Freed, A., Van Arsdale, R., Stein, S., 2010. Triggering of New Madrid seismicity by late-Pleistocene erosion. Nature 466 (7306), 608–611.

Chow, G. C., 1960. Tests of equality between sets of coefficients in two linear regressions. Econometrica 28, 3, 591–605.

Chung, W., 2002. Earthquakes along the passive margin of Greenland: Evidence for postglacial rebound control. Pure and Applied Geophysics 159 (11-12), 2567–2584.

Chung, W.-Y., Gao, H., 1997. The Greenland earthquake of 11 July 1987 and postglacial fault reactivation along a passive margin. Bulletin of the Seismological Society of America 87 (4), 1058–1068.

Clinton, J. F., Nettles, M., Walter, F., Anderson, K., Dahl-Jensen, T., Giardini, D., Govoni, A., Hanka, W., Lasocki, S., Lee, W. S., McCormack, D., Mykkeltveit, S., Stutzmann, E., Tsuboi, S., 2014. Seismic network in Greenland monitors Earth and ice system. Eos, Transactions American Geophysical Union 95 (2), 13–14.

Dahl-Jensen, T., Larsen, T. B., Voss, P. H., et al., 2010. Greenland ice sheet monitor-

ing network (GLISN): a seismological approach. Geological Survey of Denmark and Greenland Bulletin 20, 55–58.

Darbyshire, F. A., Larsen, T. B., Mosegaard, K., Dahl-Jensen, T., Gudmundsson, O., Bach, T., Gregersen, S., Pedersen, H. A., Hanka, W., 2004. A first detailed look at the Greenland lithosphere and upper mantle, using Rayleigh wave tomography. Geophysical Journal International 158 (1), 267–286.

Dziewonski, A., Chou, T.-A., Woodhouse, J., 1981. Determination of earthquake source parameters from waveform data for studies of global and regional seismicity. Journal of Geophysical Research 86 (B4), 2825–2852.

Escher, J., Pulvertaft, T., 1995. Geological map of Greenland, 1:2,500,000. Tech. rep., Geological Survey of Greenland, Copenaghen.

Gordon, R. G., 1998. The plate tectonic approximation: Plate nonrigidity, diffuse plate boundaries, and global plate reconstructions. Annual Review of Earth and Planetary Sciences 26 (1), 615–642.

Gregersen, S., 1982. Earthquakes in Greenland. Bull. Geol. Soc. Denmark 31, 11–27.

Gupta, H. K., Rao, N. P., Rastogi, B. K., Sarkar, D., 2001. The deadliest intraplate earthquake. Science 291 (5511), 2101–2102.

Gutenberg, B., Richter, C. F., 1944. Frequency of earthquakes in California. Bulletin of the Seismological Society of America 34 (4), 185–188.

Gutenberg, B., Richter, C. F., 1954. Seismicity of the Earth and related phenomena. Princeton (NJ).

Hampel, A., Hetzel, R., 2006. Response of normal faults to glacial-interglacial fluctuations of ice and water masses on Earth's surface. Journal of Geophysical Research: Solid Earth (1978–2012) 111 (B6).

Hanka, W., Saul, J., Weber, B., Becker, J., Harjadi, P., Fauzi, Group, G. S., 2010. Real-time earthquake monitoring for tsunami warning in the Indian Ocean and beyond. Natural Hazards and Earth System Science 10 (12), 2611–2622.

Hough, S. E., Armbruster, J. G., Seeber, L., Hough, J. F., 2000. On the modified Mercalli intensities and magnitudes of the 1811–1812 New Madrid earthquakes. Journal of Geophysical Research: Solid Earth (1978–2012) 105 (B10), 23839–23864.

International Seismological Centre, 2011. On-line Bulletin. Int. Seis. Cent., Thatcham,

504 United Kingdom, http://www.isc.ac.uk.
505 Jakobsson, M., Björck, S., O'Regan, M., Flodén, T., Greenwood, S. L., Swärd, H., Lif, A.,
506 Ampel, L., Koyi, H., Skelton, A., 2014. Major earthquake at the Pleistocene-Holocene
507 transition in Lake Vättern, southern Sweden. Geology 42 (5), 379–382.
508 Johnston, A. C., 1987. Suppression of earthquakes by large continental ice sheets. Nature
509 330, 467–469.
510 Larsen, T. B., Voss, P. H., Dahl-Jensen, T., Rasmussen, H. P., 2014. Earthquake swarms
511 in Greenland. Geological Survey of Denmark and Greenland Bulletin 31, 75–78.
512 Meehl, G., Stocker, T., Collins, W., Friedlingstein, P., Gaye, A., Gregory, J., Kitoh, A.,
513 Knutti, R., Murphy, J., Noda, A., Raper, S., Watterson, I., Weaver, A., Zhao, Z.-C.,
514 2007. Climate change 2007: The physical science basis, Intergovernmental Panel on
515 Climate Change. In: Solomon, S., Qin, D., Manning, M., Chen, Z., Marquis, M.,
516 Averyt, K., Tignor, M., Miller, H. (Eds.), Global Climate Projections. Cambridge
517 University Press, Cambridge, pp. 747–845.
518 Mignan, A., Woessner, J., 2012. Estimating the magnitude of completeness for earth-
519 quake catalogs. Community Online Resource for Statistical Seismicity Analysis.
520 Moon, T., Joughin, I., Smith, B., Howat, I., 2012. 21st-century evolution of Greenland
521 outlet glacier velocities. Science 336 (6081), 576–578.
522 Morgan, W. J., 1968. Rises, trenches, great faults, and crustal blocks. Journal of Geo-
523 physical Research 73 (6), 1959–1982.
524 Muir-Wood, R., 2000. Deglaciation seismotectonics: a principal influence on intraplate
525 seismogenesis at high latitudes. Quaternary Science Reviews 19 (14), 1399–1411.
526 Nettles, M., Ekström, G., 2010. Glacial earthquakes in Greenland and Antarctica. Annual
527 Review of Earth and Planetary Sciences 38 (1), 467.
528 Nettles, M., Wallace, T. C., Beck, S. L., 1999. The March 25, 1998 Antarctic plate
529 earthquake. Geophysical Research Letters 26 (14), 2097–2100.
530 Nielsen, K., Sørensen, L. S., Khan, S. A., Spada, G., Simonsen, S. B., Forsberg, R., 2014.
531 Towards constraining glacial isostatic adjustment in Greenland using ICESat and GPS
532 observations. In: Earth on the Edge: Science for a Sustainable Planet. Springer, pp.
533 325–331.
534 Olivieri, M., Clinton, J., 2012. An almost fair comparison between Earthworm and Seis-

Comp3. Seismological Research Letters 83 (4), 720–727.

Olivieri, M., Spada, G., 2013. Intermittent sea-level acceleration. Global and Planetary Change 109, 64–72.

Peltier, W., 2004. Global glacial isostasy and the surface of the Ice-Age Earth: the ICE-5G(VM2) model and GRACE. Annu. Rev. Earth Pl. Sc. 32, 111–149.

Pinna, L., Dahl-Jensen, T., 2012. Relocated local earthquakes in SE Greenland align on old geological boundaries and structures. In: EGU General Assembly Conference Abstracts. Vol. 14. p. 1635.

Quinlan, G., 1984. Postglacial rebound and the focal mechanisms of eastern Canadian earthquakes. Canadian Journal of Earth Sciences 21 (9), 1018–1023.

Rydelek, P. A., Sacks, I. S., 1989. Testing the completeness of earthquake catalogues and the hypothesis of self-similarity. Nature 337 (6204), 251–253.

Sauber, J. M., Molnia, B. F., 2004. Glacier ice mass fluctuations and fault instability in tectonically active southern Alaska. Global and Planetary Change 42 (1), 279–293.

Schrama, E. J., Wouters, B., 2011. Revisiting Greenland ice sheet mass loss observed by GRACE. Journal of Geophysical Research 116 (B2).

Schulte, S. M., Mooney, W. D., 2005. An updated global earthquake catalogue for stable continental regions: reassessing the correlation with ancient rifts. Geophysical Journal International 161 (3), 707–721.

Shearer, P. M., Stark, P. B., 2012. Global risk of big earthquakes has not recently increased. Proceedings of the National Academy of Sciences 109 (3), 717–721.

Sørensen, L. S., Simonsen, S. B., Nielsen, K., Lucas-Picher, P., Spada, G., Adalgeirsdottir, G., Forsberg, R., Hvidberg, C., 2011. Mass balance of the Greenland ice sheet (2003-2008) from ICESat data–the impact of interpolation, sampling and firn density. Cryosphere 5 (1), 173–186.

Spada, G., Ruggieri, G., Sørensen, L., Nielsen, K., Melini, D., Colleoni, F., 2012. Greenland uplift and regional sea level changes from ICESat observations and GIA modelling. Geophysical Journal International 189 (3), 1457–1474.

Spada, G., Yuen, D., Sabadini, R., Boschi, E., 1991. Lower-mantle viscosity constrained by seismicity around deglaciated regions. Nature 351 (6321), 53–55.

Steffen, R., Eaton, D. W., Wu, P., 2012. Moment tensors, state of stress and their relation

566 to post-glacial rebound in northeastern Canada. Geophysical Journal International
567 189 (3), 1741–1752.
568 Steffen, R., Wu, P., Steffen, H., Eaton, D. W., 2014a. The effect of earth rheology and ice-
569 sheet size on fault slip and magnitude of postglacial earthquakes. Earth and Planetary
570 Science Letters 388, 71–80.
571 Steffen, R., Wu, P., Steffen, H., Eaton, D. W., 2014b. On the implementation of faults
572 in finite-element glacial isostatic adjustment models. Computers & Geosciences 62,
573 150–159.
574 Stein, S., Mazzotti, S., 2007. Continental intraplate earthquakes: science, hazard, and
575 policy issues. Vol. 425. Geological Society of America, Colorado.
576 Stein, S., Sleep, N. H., Geller, R. J., Wang, S.-C., Kroeger, G. C., 1979. Earthquakes
577 along the passive margin of Eastern Canada. Geophysical Research Letters 6 (7),
578 537–540.
579 Sykes, L. R., 1978. Intraplate seismicity, reactivation of preexisting zones of weakness,
580 alkaline magmatism, and other tectonism postdating continental fragmentation. Re-
581 views of Geophysics 16 (4), 621–688.
582 Sykes, L. R., Sbar, M. L., 1974. Focal mechanism solutions of intraplate earthquakes and
583 stresses in the lithosphere. In: Kristjansson, L. (Ed.), Geodynamics of Iceland and the
584 North Atlantic Area. Springer, pp. 207–224.
585 Turcotte, D. L., Schubert, G., 2002. Geodynamics. Cambridge University Press, Cam-
586 bridge.
587 Tushingham, A., Peltier, W., 1991. Ice-3g: A new global model of Late Pleistocene
588 deglaciation based upon geophysical predictions of post-glacial relative sea level
589 change. Journal of Geophysical Research: Solid Earth (1978–2012) 96 (B3), 4497–
590 4523.
591 Velicogna, I., Wahr, J., 2005. Greenland mass balance from GRACE. Geophysical Re-
592 search Letters 32 (18).
593 Walter, F., Clinton, J. F., Deichmann, N., Dreger, D. S., Minson, S. E., Funk, M., 2009.
594 Moment tensor inversions of icequakes on Gornergletscher, Switzerland. Bulletin of
595 the Seismological Society of America 99 (2A), 852–870.
596 Walter, F., Olivieri, M., Clinton, J. F., 2013. Calving event detection by observation of

seiche effects on the Greenland fjords. Journal of Glaciology 59 (213), 162–178.

Wessel, P., Smith, W. H. F., 1998. New, improved version of generic mapping tools released. EOS 79, 579.

Winer, B. J., 1962. Statistical principles in experimental design. McGraw-Hill (New York).

Woessner, J., Wiemer, S., 2005. Assessing the quality of earthquake catalogues: Estimating the magnitude of completeness and its uncertainty. Bulletin of the Seismological Society of America 95 (2), 684–698.

Wu, P., Johnston, P., 2000. Can deglaciation trigger earthquakes in N. America? Geophysical Research Letters 27 (9), 1323–1326.

Table 1: Fault mechanisms for the largest recorded earthquakes in Greenland for the time period 1951–2012.

Date	Lat	Lon	Depth	M	Strike	Dip	Slip	Strike	Dip	Slip	Moment M_o
	deg	deg	km		deg	deg	deg	deg	deg	deg	$\times 10^{24}$ dyne cm
1971/11/26	79.43	-18.00	2	5.1	63	52	-51	190	52	-129	2.00
1987/07/11	82.23	-17.55	5	5.5	27	50	-43	148	59	-131	1.75
1993/08/10	83.06	-27.5	11	5.4	127.4	56.9	-115.8	348.9	41.0	56.3	1.27
1998/10/14	60.71	-44.05	5	5.1	61.6	58.0	-95.5	251.9	32.4	-81.3	0.57

Table 2: Greenland sectors and corresponding best fitting model. The uncertainties on the rates correspond to 1σ.

Sector	M_c	Starting time	Number of events	best-fitting function	rate before CP events/year	CP year	rate after CP events/year
Greenland	4.0	1969	75	bilinear	1.33 ± 0.02	1993.54	1.83 ± 0.05
North (N)	4.0	1976	30	bilinear	0.93 ± 0.04	1993.70	0.49 ± 0.03
Southeast (Se)	4.0	2002	7	linear			
West (W)	3.9	1999	14	linear			

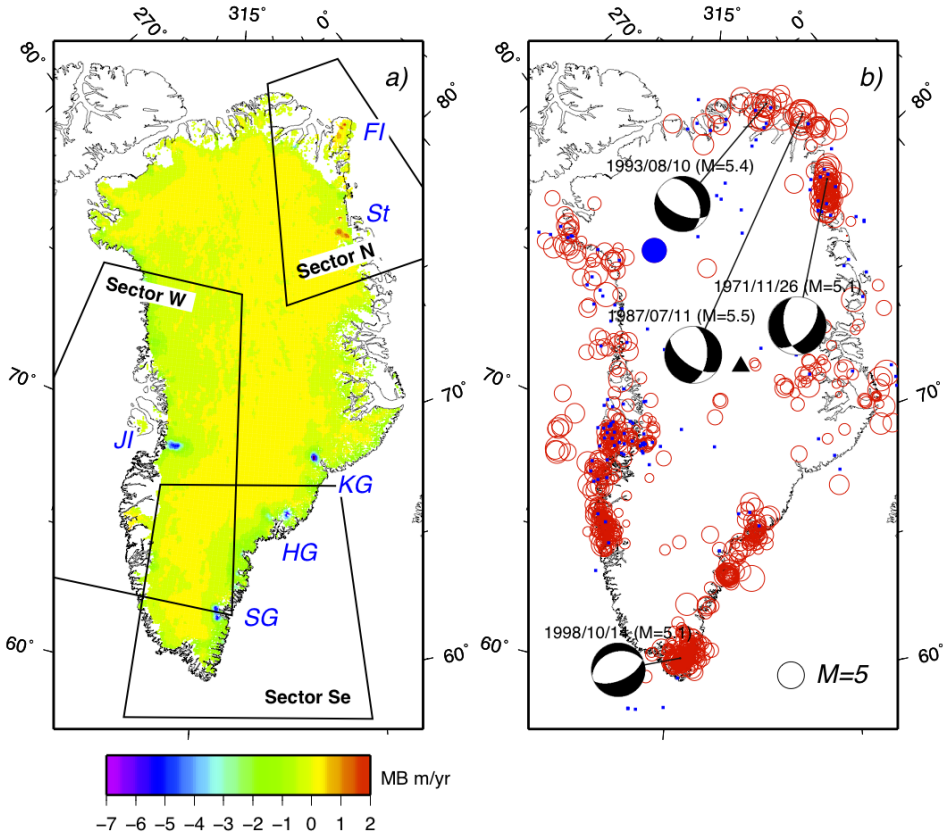

Figure 1: (a): Mass balance of the GrIS for period 2003–2008 according to model M3 of Sørensen et al. (2011) (in units of meter yr^{-1}) and location of the major sources of ice loss (JI: Jakobshavn Isbræ, KG: Kangerdlugssuaq Glacier, HG: Helheim Glacier, SG: Southeast Glaciers, FI: Flade Isblink, St: Storstrømmen). Sectors W, Se and N mark three areas of intense seismicity in the west, the southeast and the north. (b): Seismicity of Greenland in the time frame 1951–2012. Black dots: earthquakes of unknown magnitude; red circles: earthquakes of known magnitude scaled by size. The only four known focal mechanisms are also shown in lower hemisphere projection. A blue dot locates the largest earthquake that occurred inland ($M = 4.6$). The black triangle indicates the seismic station GE.SUMG (Summit).

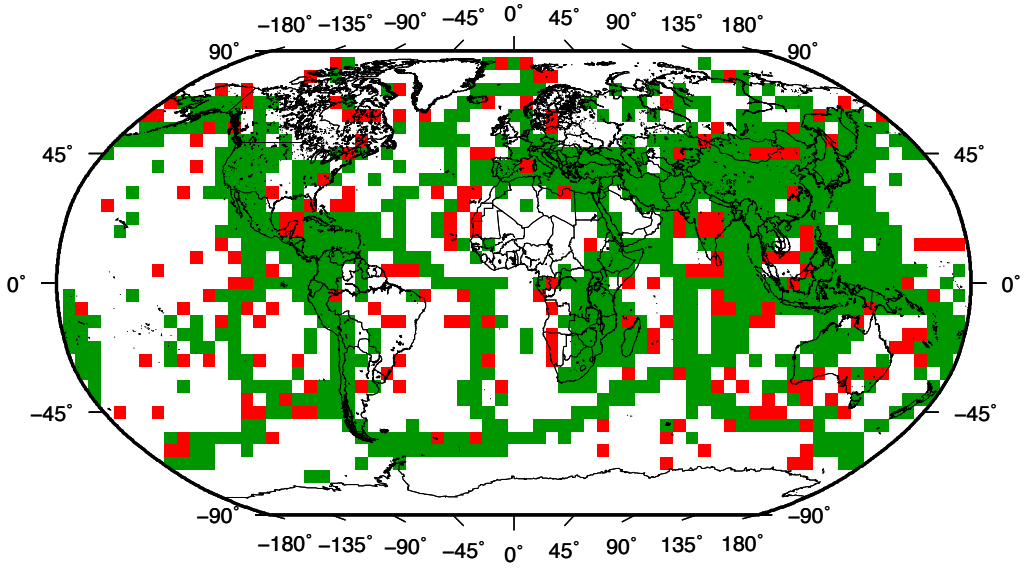

Figure 2: Global seismicity distribution ($M \geq 5$, $h < 30$ km) according to the ISC database. Red pixels show areas where earthquakes only occurred during 1988–2011, green ones mark those showing seismicity both before and after 1988.

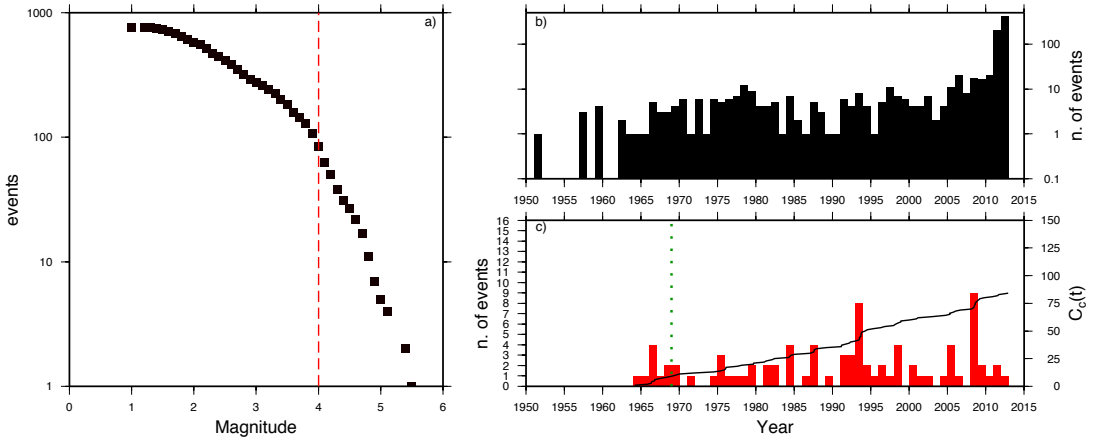

Figure 3: Summary of the distribution of seismicity recorded in Greenland. (a): Gutenberg-Richter relation in which the cumulative number of events exceeding magnitude M is plotted against M on a lin-log scale. Red dashed line marks the selected magnitude of completeness $M_c = 4.0$. (b): number of events recorded every year across Greenland on lin-log scale. (c): Cumulative function $C_c(t)$ (thick curve), and, in red, histogram of the number of events (bin-width = 2 years). Both refer to earthquakes with magnitude $M > M_c$. A dashed green line marks the starting time for the validity of M_c.

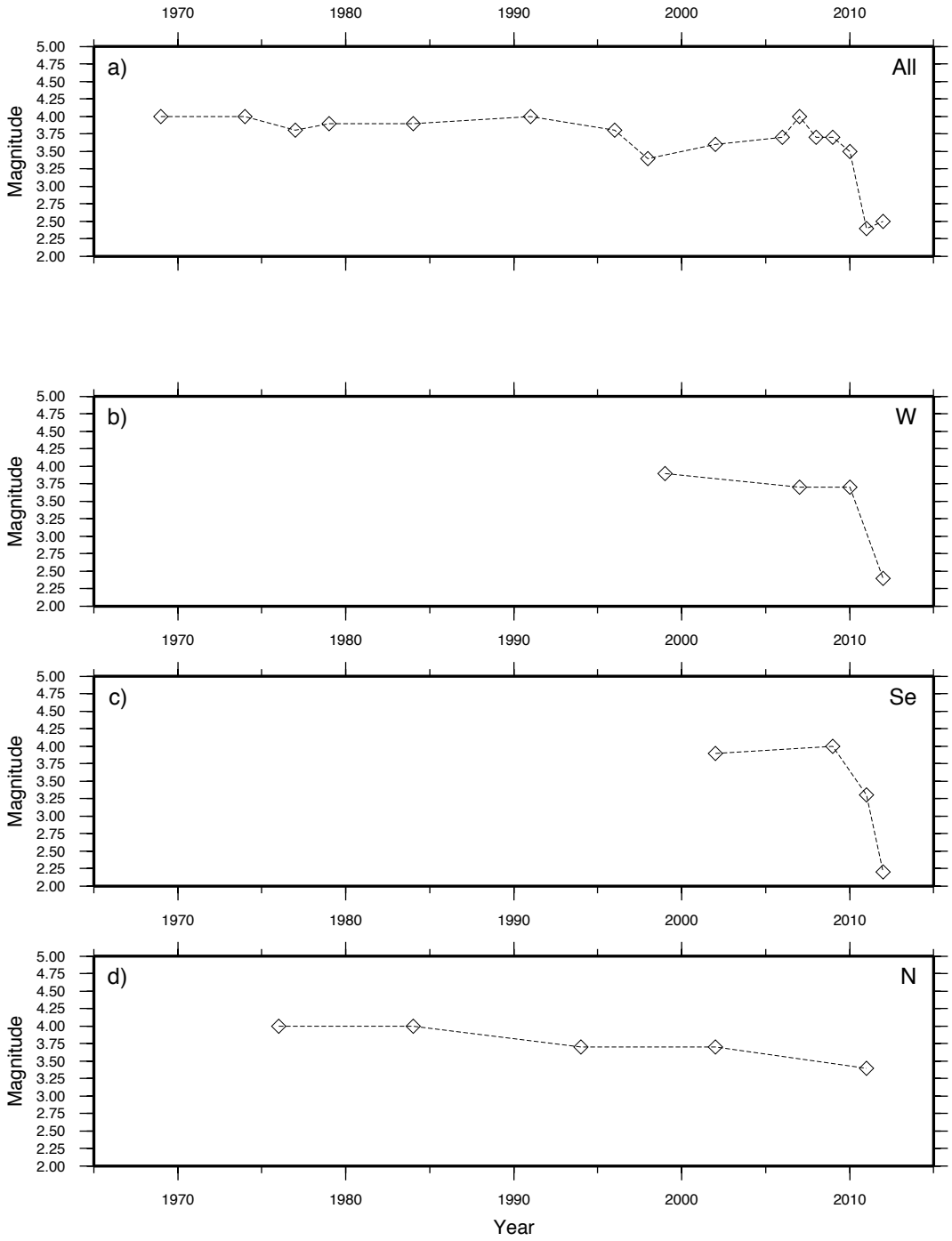

Figure 4: M_c as a function of time. Each diamond represents one estimate of M_c for a set of 50 events. Time stamp assigned to each M_c corresponds to the median year of the subset. (a): Evolution of M_c for the entire catalogue; (b): same as for frame (a) but restricted to sector W; (c): sector Se; (d): sector N. The different starting time of each function depends on the availability of detected events that varies from sector to sector, as described in the body of the manuscript.

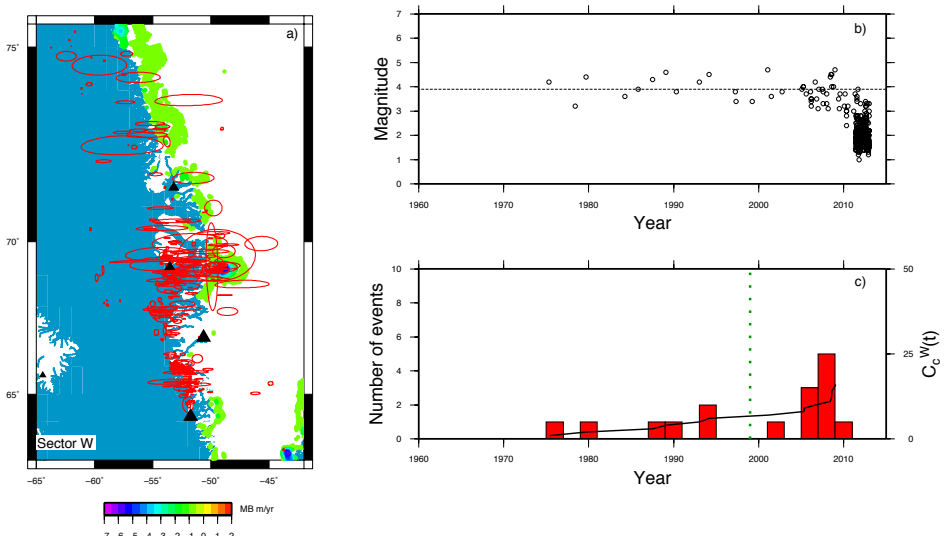

Figure 5: Summary of the recorded earthquake activity in sector W (see Figure 1). (a): map of the area (blue is water, white is land), color scale indicate the rate of mass change (we only display pixels where the rate of mass balance exceeds 0.5 Gt yr^{-1} in modulus). Earthquake locations uncertainties are represented by means of the error ellipsoids as reported by the ISC catalogue. Black triangles identify seismic stations. (b): earthquake magnitude as a function of time. (c): histogram for the number of earthquakes recorded every year; in red events with $M \geq M_c$ in linear scale. Thick line represents the cumulative function $C_c^W(t)$ as described in Sections 3.1 and 3.2. Dashed vertical line marks the starting time for the validity of M_c as from Table 2.

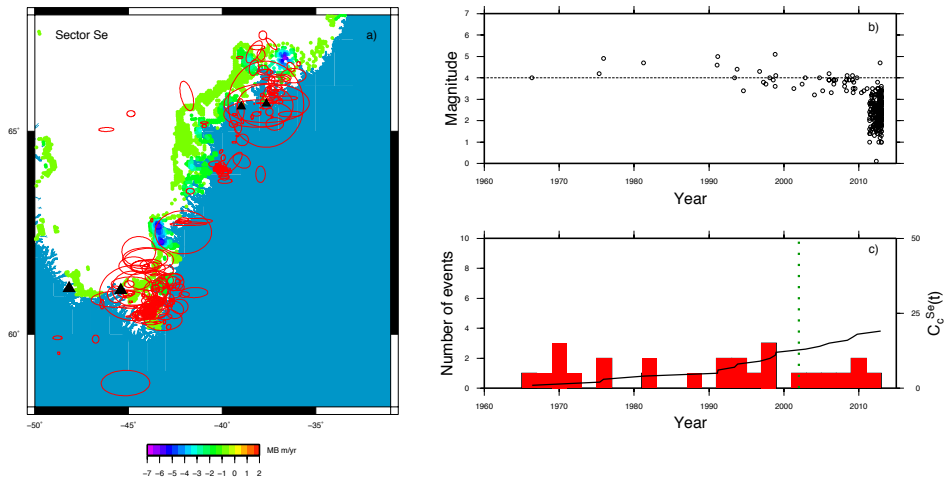

Figure 6: The same as in Figure 5 for sector Se.

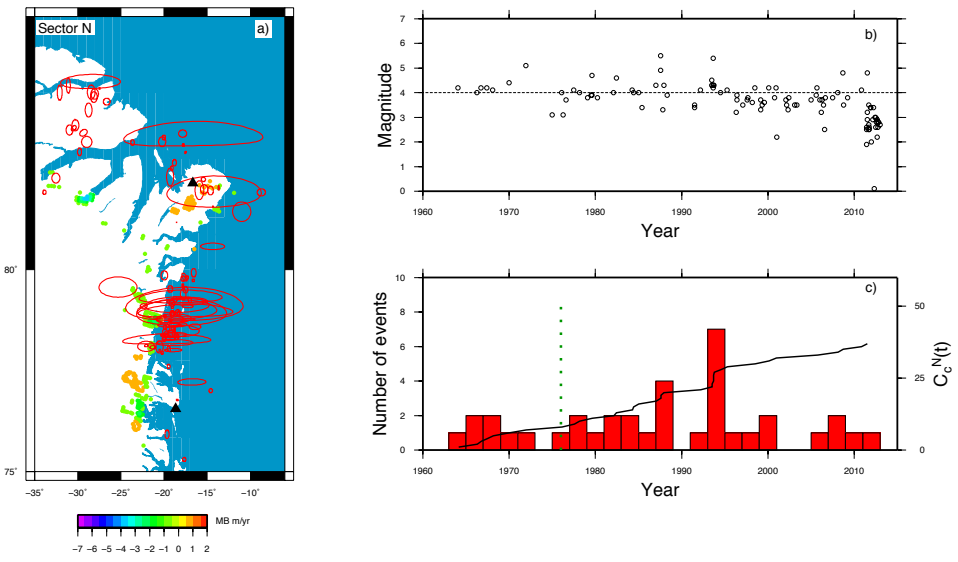

Figure 7: The same as in Figure 5 for sector N.

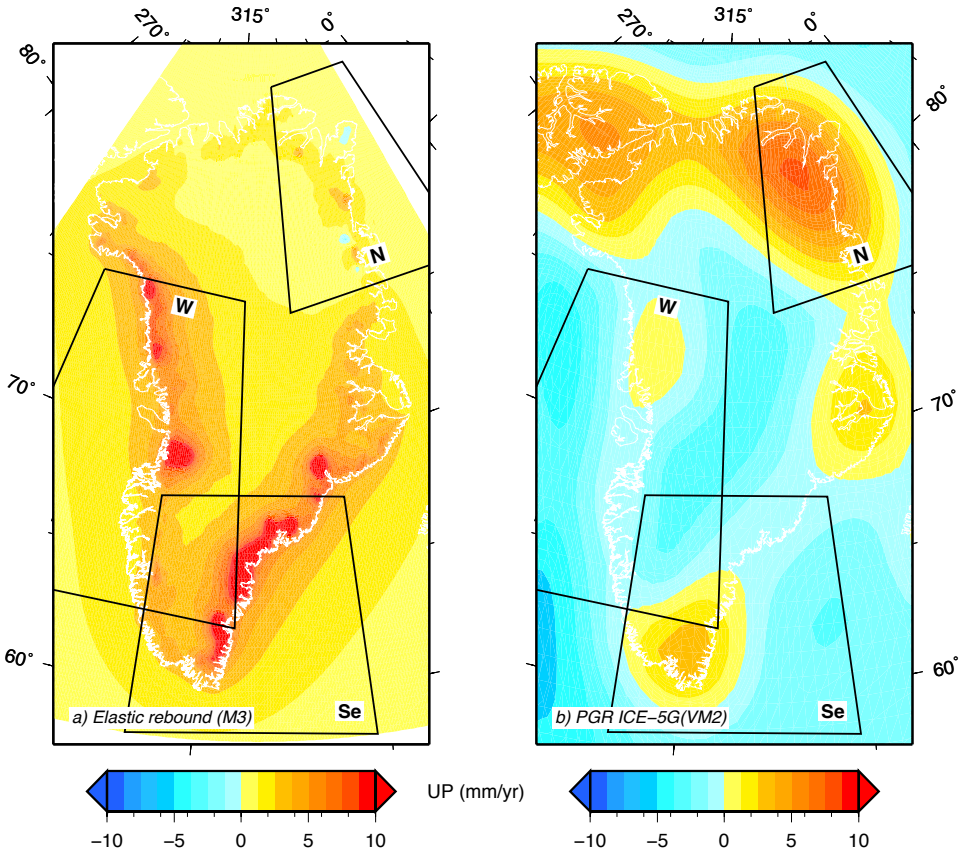

Figure 8: Average rate of vertical displacement for the period 2003–2008 across Greenland. (a): contribution of the ER in response to current melting according to the mass balance M3 shown in Figure 1a; (b): PGR component of the uplift rate according to the ICE-5G(VM2) model of Peltier (2004).